Organic chemistry influences the observed seasonal cycle of molecular oxygen on Mars

Benjamin M. Taysum,[1,2*] Paul I. Palmer,[1,2]

[1]School of GeoSciences, University of Edinburgh, Edinburgh, UK
[2]Centre for Exoplanet Science, University of Edinburgh, Edinburgh, UK

[*]To whom correspondence should be addressed; E-mail:Ben.Taysum@ed.ac.uk.

This PDF file includes:

Materials and Methods

Supplementary Text

Figs. S1 to S4

References

1 Materials and Methods

1.1 Tangent Linear Model and Adjoint Proofs

We use the adjoint of the tangent linear model (TLM) to determine the sensitivity of trace gas A at time t to changes in photochemically-related gases at prior times. Here, we document the TLM and its adjoint and provide an assessment of its accuracy.

Fully Integrated Model Equations

The 1-D model performs time-dependent calculations of tracer mass mixing ratios (MMRs) across discrete altitude steps, denoted by $\vec{PQ}$, using Equation 1.

$$\frac{\partial PQ_{i,l}}{\partial t} = P_{i,l} - L_{i,l} - \frac{\partial \phi_{i,l}}{\partial z} \tag{1}$$

Vertical diffusion, determined by vertical diffusive fluxes $\phi_{i,l}$ of species i at model layer l within the 1-D photochemistry model, is governed by the classical diffusion equation (*1*); we refer the reader to (*2*) for further details about the turbulent mixing routines. Photochemistry routines calculate the production and loss terms, $\mathrm{P}_{i,l}$ and $\mathrm{L}_{i,l}$ respectively, of each chemistry species.

Model calculations are discretised across space and time in altitude and physical timesteps denoted by Δz and Δt_p, respectively. We use 48 physical time steps (1800 s) per Martian sol, and altitude steps of less than 0.5 km below an altitude of 2 km that progressively increase to 10 km above an altitude of 20 km, following our previous work (*3*)

The stiffness of the discretised photochemistry equations is decreased by using a chemistry sub-timestep Δt_c of 600 s, corresponding to three sub-timesteps per physical timestep (*3*). The discretised form of Equation 1 is denoted by the 1-D model function F_{1D}:

$$\frac{\Delta PQ_{i,l}}{\Delta t_p} = F_{1D}(\vec{PQ}) = \Delta t_p^{-1}\Big(\Delta PQ_{i,l}^{Chem}(\vec{PQ}) - \Delta PQ_{i,l}^{Diff}(\vec{PQ})\Big), \tag{2}$$

where Δt_p denotes the timestep of the perturbation. Below we devote individual sections to the details of the diffusion (*Diff*) and chemistry (*Chem*) components.

Tangent Linear Model

The TLM of a mathematical function, such as $\mathrm{F}_{1D}(\vec{PQ})$ (Equation 2), is a linearized version of the perturbation $\Delta\vec{PQ}^{t}$ around the control state $\vec{PQ}_{C}^{t}$. The TLM is calculated using the Gateaux differentiation of Equation 2, which is first rearranged to form Equation 3:

$$G(\vec{PQ}) = \frac{\Delta\vec{PQ}}{\Delta t_p} - F_{1D}(\vec{PQ}) = 0 \quad , \tag{3}$$

First, we define a control model run, initialised with a tracer MMR vector $\vec{PQ}^{t=0} = \vec{PQ}_{C}^{t=0}$, and a model run with an initial MMR vector $\vec{PQ}^{t=0} = \vec{PQ}_{P}^{t=0}$ which is a perturbation of the control state such that $\vec{PQ}_{P}^{t} = \vec{PQ}_{C}^{t} + \vec{PQ}^{t}$". These two model runs allows us to use the Gateaux expansion (Eq. 3) for the perturbed state around the control state, defined by Equation 4 and 5, for a vector of scalars $\vec{\lambda}$:

$$G(\vec{PQ}_{C} + \vec{PQ}") - G(\vec{PQ}_{C}) = \Delta G \tag{4}$$

$$\Delta G = \frac{d}{d\vec{\lambda}} G(\vec{PQ}_{C} + \vec{\lambda}\vec{PQ}") \mid_{\lambda_\forall = 0} \; = 0 \tag{5}$$

Inserting Equation 3 into 5, and performing a substitution of variables with $\vec{X} = \vec{PQ}_{C} + \vec{\lambda}\vec{PQ}$" results in Equations 6 and 7. This expression is then evaluated for values of $\lambda_\forall = 0$ to produce the TLM equation displayed in Equation 8,

$$\frac{d}{d\lambda}\Big[\frac{\Delta(\vec{X})}{\Delta t_p} - F_{1D}(\vec{X})\Big] \mid_{\lambda_\forall = 0} \; = 0 \tag{6}$$

$$\frac{\Delta\vec{PQ}"}{\Delta t_p} - \vec{PQ}" \frac{\partial F_{1D}(\vec{X})}{\partial\vec{X}} \mid_{\lambda_\forall = 0} \; = 0 \tag{7}$$

$$F_{TLM}(\vec{PQ}") \equiv \frac{\Delta\vec{PQ}"}{\Delta t_p} = \vec{PQ}" \frac{\partial F_{1D}(\vec{PQ})}{\partial\vec{PQ}} \mid_{C}, \tag{8}$$

where C denotes the partial derivative across the 1-D model control state. The TLM of the 1-D photochemistry submodule linearizes the discrete model equations (2) that are derived from (1)

to enable a greater degree of accuracy when we compare results between the fully integrated 1-D model with calculations from its TLM.

Discretising Equation 8 across the 1-D model timesteps enables the TLM to evaluate the evolution of perturbations to the MMR vector in parallel with the control model run by using variable values that appear in the control state, displayed in Equation 9:

$$\vec{PQ}^{t+1}{}" = \vec{PQ}"^{t} + \frac{\Delta \vec{PQ}"}{\Delta t_p}\Delta t_p \quad , \tag{9}$$

which can be rearranged to highlight its structure as a matrix equation (Equation 10):

$$\vec{PQ}^{t+1}{}" = \left(\mathbf{I} + \Delta t_p \frac{\partial F_{1D}(\vec{PQ})}{\partial \vec{PQ}} \mid_C \right) \vec{PQ}"^{t} = \mathbf{A}_t \times \vec{PQ}^{t}", \tag{10}$$

where the TLM matrix, $\mathbf{A}_t$, is constructed from control run MMR values at timestep t. Multiplication by the perturbation vector $\vec{PQ}^{t}$ advances the perturbed state to the subsequent 1-D model timestep.

The MMR perturbation vector $\vec{PQ}"$ is of size N, and holds the perturbation in units of kg/kg of all I trace gas species and across all L model layers. So that for the TLM used in this work, the perturbation vectors are of length $N = L \times I = 25 \times 27 = 675$. Element $[(i \times l), (j \times m)]$ of the TLM matrix $\mathbf{A}_t$ denotes the gradient of the MMR of tracer species *i* at model layer *l* with respect to the MMR of tracer species *j* at model layer *m* at timestep t. This creates a matrix of size $N \times N$, where N=675 in our work. Extending Equation 10 to some arbitrary initial timestep provides an expression for the transition matrix, $\mathbf{R}$:

$$\vec{PQ}^{N}{}" = \prod_{t=-N}^{0} \mathbf{A}_{-t} \vec{PQ}^{0}{}" \equiv \mathbf{R}_N \vec{PQ}^{0}{}" \quad . \tag{11}$$

Comparison of the 1-D Photochemical Model and its TLM

We assess the accuracy of the TLM by comparing the perturbations to the control state integrated forward in time by the TLM with the same perturbation predicted by two separate runs

of the fully integrated 1-D model. If we define these runs as a function of initial conditions, where $\vec{PQ}_C^{t=0}$ is the initial control state and $\vec{PQ}_P^{t=0} = \vec{PQ}_C^{t=0} + \vec{\lambda}\vec{PQ}_C^{t=0}$ is the perturbed initial conditions for a vector of scalars $\vec{\lambda}$, the validity test is given by:

$$\lim_{\lambda_n \longrightarrow 0,\ \forall 1 \leq n \leq N} F_{1D}(\vec{PQ}_C^{t=0} + \vec{\lambda}\vec{PQ}_C^{t=0}) - F_{1D}(\vec{PQ}_C^{t=0}) = F_{TLM}(\vec{\lambda}\vec{PQ}_C^{t=0}) \quad . \tag{12}$$

The TLM model code uses double precision floating point mathematics whereas the 1-D photochemistry operates in single precision. We take these differences into account in our validity assessment by using a tolerance:

$$\frac{PQ_{i,l|P}^t - PQ_{i,l|C}^t}{PQ_{i,l|C}^t} \geq 1 \times 10^{-6} \quad , \tag{13}$$

where all variables are as previously defined.

Figure S1 shows four examples in which we compare the results from a brute-force perturbation of the 1-D model photochemistry, e.g. perturbing H_2O_2 in model levels 8–10, with the TLM approximation given by Equation 10. The magnitude of the perturbation λ is given by:

$$\lambda = \frac{m_{i,l,P}^{t=0}}{m_{i,l,Control}^{t=0}} - 1, \tag{14}$$

where i denotes the chemical species being perturbed, l denote the model vertical levels at which the species is perturbed. We compare mass mixing ratios from the two methods of perturbation over 144 physical timesteps (=three sols).

Generally, we find a strong linear relationship between the 1-D model and the TLM approximation, with slopes typically within 3% of the unit target value and Pearson correlation coefficients $\simeq$0.95 for a range of λ values. Small perturbations of H, OH, and HO_2 smaller than the precision criterion defined above are propagated by the TLM approximation but are not captured by the 1-D model that uses single precision.

Based on these calculations we conclude that our TLM represents a good linearisation of the fully integrated 1D chemistry model developed in (*3*) despite differences in the two models'

machine precision. The TLM enables us to develop high quality sensitivity analyses regarding the atmospheric state of Mars, and provides the basis of an accurate adjoint data assimilation scheme developed from the TLM.

1-D Photochemistry Adjoint

The adjoint model approaches takes advantage of the *adjoint property*, defined as $(\vec{x}, \mathbf{A}\vec{y}) = (\mathbf{A}^T\vec{x}, \vec{y})$. This property holds for a linear map $\mathbf{A}$ from vector $\vec{x}$ to vector $\vec{y}$, and the *adjoint* of this linear map $\mathbf{A}^T : \vec{y} \longrightarrow \vec{x}$, in which T denotes the matrix transpose.

The adjoint model is used to produce a gradient of sensitivities for a selected forecast element $J = PQ^{\Omega}_{i,l}$, representing the MMR of tracer *i* at model layer *l* at the desired forecast timestep *t* = Ω. The change in this desired element, ΔJ, is quantified by Equation 15. The change in the studied forecast element is the product of a) the change in MMR of tracer *i* at model layer *l* at timestep $0 \leq t \leq N$, $\Delta PQ^{\Omega}_{a,b}$ and b) the sensitivity of the forecast element to a change in the MMR, $\hat{J}^t_{a,b}$:

$$\Delta PQ^{\Omega}_{i,l} \equiv \Delta J = \sum_{a=1}^{I}\sum_{b=1}^{L} \frac{\partial J}{\partial PQ_{a,b}}^{t} \Delta PQ^{t}_{a,b} \equiv \sum_{a=1}^{I}\sum_{b=1}^{L} \hat{J}^t_{a,b}\Delta PQ^{t}_{a,b} \quad . \tag{15}$$

The adjoint of the 1-D photochemistry model is used to calculate the sensitivity vectors $\hat{J}$ across all prior model timesteps through the use of Equation 16:

$$\hat{J}^{t-1} = \mathbf{A}^T_{t-1}\hat{J}^t \quad . \tag{16}$$

which uses the transpose of the TLM matrices $\mathbf{A}_t$ and the adjoint property, defined above, to iterate the model *backwards* through time to mathematically quantify how sensitive the desired forecast element J is to the entire chemical constituency of the 1-D model control state at all previous model timesteps. Using the adjoint approach enables us to address questions such as "what changes in the photochemistry help explain the discrepancies between O_2 measurements collected by the Curiosity Rover and those predicted by GCM models (*4*)?"

First, we need to initialize the adjoint model equation (Equation 16) at the forecast time $t = N$. For a singular forecast aspect J taken at time $t = \Omega$, the only way a perturbation at time $t = \Omega$ could impact the value of J is if the perturbation were to be made to the aspect itself. The initial sensitivity vector $\hat{J}^{t=\Omega}$ will only have one non-zero element which will correspond to the location of the forecast aspect in the MMR perturbation vector $\vec{PQ}$". This non-zero value will be unity, due to this sensitivity element being equal to the partial derivative of J with itself, $\partial J/\partial J = 1$. As the sensitivity vectors are gradients of MMRs with respect to MMRs in this work, they can be regarded as dimensionless scale factors.

Evaluating the Adjoint Property of the TLM Matrix

The adjoint model is based upon the concept of the Adjoint Property:

$$(\vec{a}, \mathbf{A}\vec{b}) = (\mathbf{A}^T\vec{a}, \vec{b}) \quad , \tag{17}$$

which must be satisfied for Equation 16 to be valid.

In Figure S2, both sides of Equation 17 are calculated using TLM matrices to produce transition matrices $\mathbf{R}_t$, adjoint calculated sensitivity vectors $\vec{\hat{J}}_t$ using Equation 16, and initial perturbation vector $\vec{x'}^{t=0}$ from the same examples shown by Figure S1. The values of each side are calculated across 240 model timesteps (= 5 sols), and their differences calculated and displayed. Across all timesteps in all cases, the two sides of the adjoint property vary only at machine precision levels, highlighting that the adjoint property is valid for the TLM constructed here. This is an important test for the adjoint of our TLM because $\mathbf{R}_{N-1}^T$, the transpose of the transition matrix, does not necessarily equal $\mathbf{R}_{N-1}^{-1}$, the inverse of the transition matrix.

Temporal Invariance of Adjoint Results

If we take Equation 10 at the studied forecast time $t = N$, it can then be extended to examine the perturbed MMR vector at the forecast time $\vec{PQ}^N$" to the initial perturbed state $\vec{PQ}^0$" to

construct the transition matrix $\mathbf{P}_N$ (wquation 11).

If we rewrite Equation 15 using inner product notation and then insert Equation 11 we can use the adjoint property as a test of the reliability of the 1-D model adjoint method. Equation 18 shows that the perturbations in the initial MMR vector $\vec{PQ}^{0}$" result in the perturbation to the desired forecast element $\Delta J_N = PQ_{i,l}^N$ through the sensitivities calculated at the initial time $\hat{J}_{t=0}$:

$$\Delta J_N = (\mathbf{R}_N^T \vec{\hat{J}}_N, \vec{PQ}^{t_0}") \tag{18}$$

It then follows that as the transition matrix $\mathbf{R}^t$ can be defined at any desired timestep where $0 \leq t \leq N$, the value of ΔJ_N will be temporally invariant and can be evaluated at any model timestep.

Figure S3 examines the temporal invariance in the second example case study from Figure S1 for which O_2 has been perturbed across layers 1 and 2 with a magnitude of λ = 10^{-1}. We chose a forecast timestep of N = 144 (=3 sols). For all tracers i at layers l that experience a perturbation greater than 10^{-16} kg/kg in the 1-D model at this forecast timestep, we calculate the adjoint sensitivities of tracer i at layer l and the TLM perturbation vectors at each prior timestep $0 \leq t_0 < N$. We then calculate the adjoint perturbation values with corresponding values from the 1-D model, $\Delta J_N^{i,l}$. Figure S3 shows that for all trace gas species with perturbations at timestep N = 144 greater than 10^{-16} kg/kg, the adjoint method, using TLM calculated perturbations and adjoint calculated sensitivities, regularly achieves differences of less than 1%. We find these discrepancies are approximately invariant with respect to the backtrace timestep t_0. This calculation highlights that the adjoint is temporally invariant, yielding consistent results from all model timesteps.

2 Supplementary Text

2.1 Organic Products from the Accelerated Organic Chemical Network

Figure S4 shows the volume mixing ratio profiles (mol/mol) and column abundances (kg/kg) of CH_4 oxidation products calculated by the 1-D model when we force the photochemical lifetime of CH_4 below 400 m to be one hour. These include formaldehyde (HCHO), methyl hydroperoxide (CH_3OOH), formic acid (HCOOH), methanol (CH_3OH), methanediol ($HOCH_2OH$), and hydromethyl hydroperoxide ($HOCH_2OOH$). Where possible, we also show the theoretical detection limits for the Trace Gas Orbiter (TGO) NOMAD (Nadir and Occultation for MArs Discovery) and ACS (Atmospheric Chemistry Suite) spectrometer suites (*5, 6*).

The ACS low and high dust limits correspond to limits where the optical opacity of the atmosphere is set to $\tau = 0.2$ and 2, respectively. The detection limits in ACS solar occultation (SO) channels in these two dust conditions are 0.17 ppb and 1.7 ppb, respectively, which occur at approximately 2.5 km altitudes in the 1-D model. The NOMAD SO channels are more sensitive, with signal to noise ratios of 2000 and 3000 that correspond to detection limits lower to 0.04 and 0.03 ppb, respectively. These are reached at altitudes of 2.5–5 km throughout the Martian year, as calculated in the 1-D model.

NOMAD is the only TGO spectrometer with the capacity to observe column abundances of formaldehyde (HCHO). The limb nadir and solar Occultation (LNO) infrared spectrometer within the NOMAD suite and the ultraviolet/visible (UVIS) spectrometers have detection limits of 150 ppb and 16 ppb respectively, and the 1-D model calculates column abundances with magnitudes of 0.1 ppb, well below the detection limits.

CH_4 has theoretical detection limits provided by NOMAD and ACS (*5, 6*). ACS low and high dust condition limits in SO channels are 0.11 ppb and 0.97 ppb, respectively. The lower limit is reached at altitudes of roughly 5 km when the 1-D model is provided with a uniformly

distributed CH_4 VMR as prescribed by SAM (*7*) below altitudes of 400 m, and the higher limit in the high dust conditions is not achieved by the 1-D model at any altitude. The NOMAD solar occultations have detection limits of 0.025 ppb and 0.02 ppb with SNRs of 2000 and 3000, encountered at altitudes of 5–7.5 km. The NOMAD's UVIS spectrometer has theoretical column abundance detection limits of 11 ppb, which are not exceeded in our photochemical calculations.

Noting the topography of Gale Crater, the crater floor lies approximately 4.4 km below the Martian "sea level," the mean elevation across Mars' equator. Observed optical opacities do not commonly drop below $\tau = 0.3$ across the Martian year at Gale Crater (*8*). These factors, coupled with the low altitudes that the TGO detection limits are reached for HCHO and CH_4 in the 1-D model, implies that a highly reactive atmospheric environment for CH_4 could exist below the PBL at Gale Crater that contributes to the O_2 seasonal cycle whilst remaining undetectable by satellite observations in solar occultation and nadir modes.

3 Figures

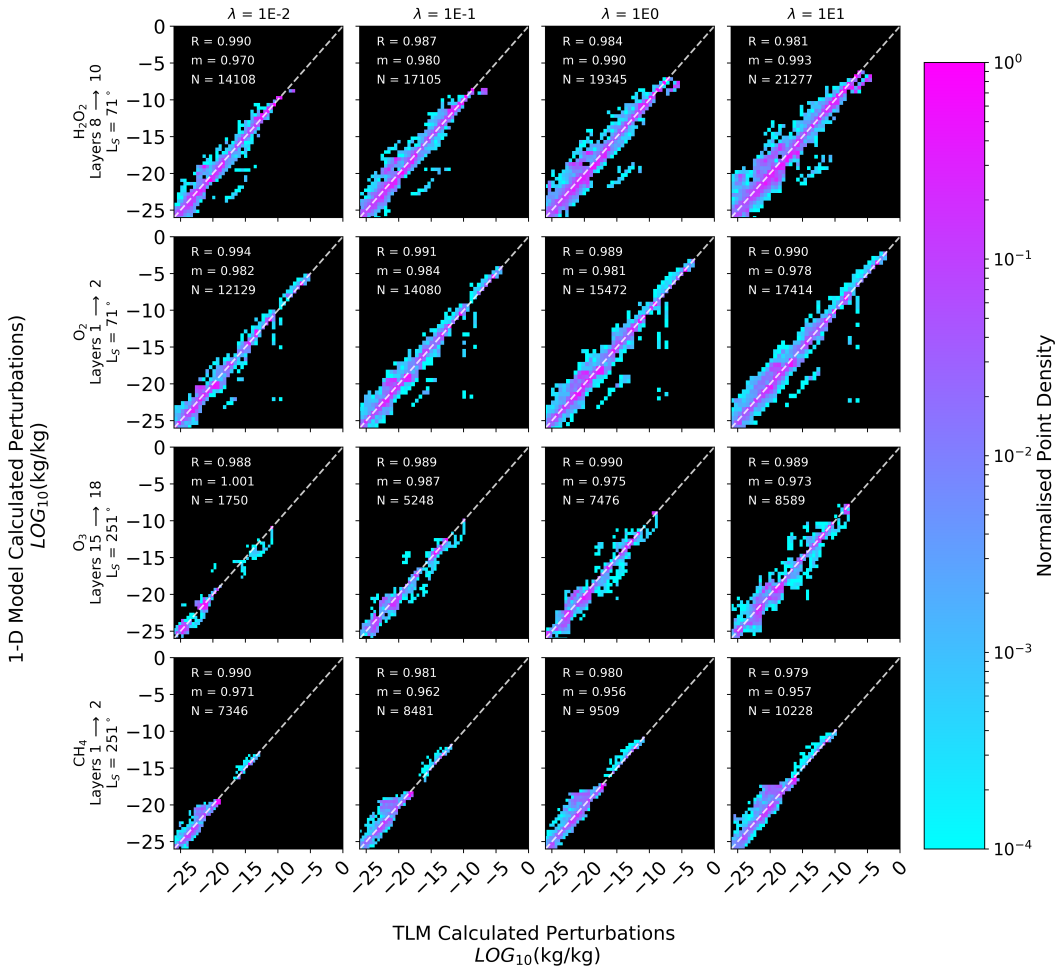

Figure S1: Comparisons of perturbations to all 27 trace gas species within the 1-D model calculated by the fully integrated 1-D model and those calculated by the TLM approximation. Initial perturbations are detailed on the left hand side, with perturbation magnitudes λ labeled on top of each column. Perturbations are tracked and plotted across 5 Martian sols (240 timesteps). The initially perturbed tracer species (i), the model layer (l) the initial perturbation is made at within the model, and the solar longitude of the cases are detailed on the y-axis. The initial magnitude of the perturbation, $\lambda = \frac{m^{t=0}_{i,l,P}}{m^{t=0}_{i,l,Control}} - 1$, is detailed along the top of the x-axis. R = Correlation coefficient, m = gradient of line of best fit, N = total number of data points.

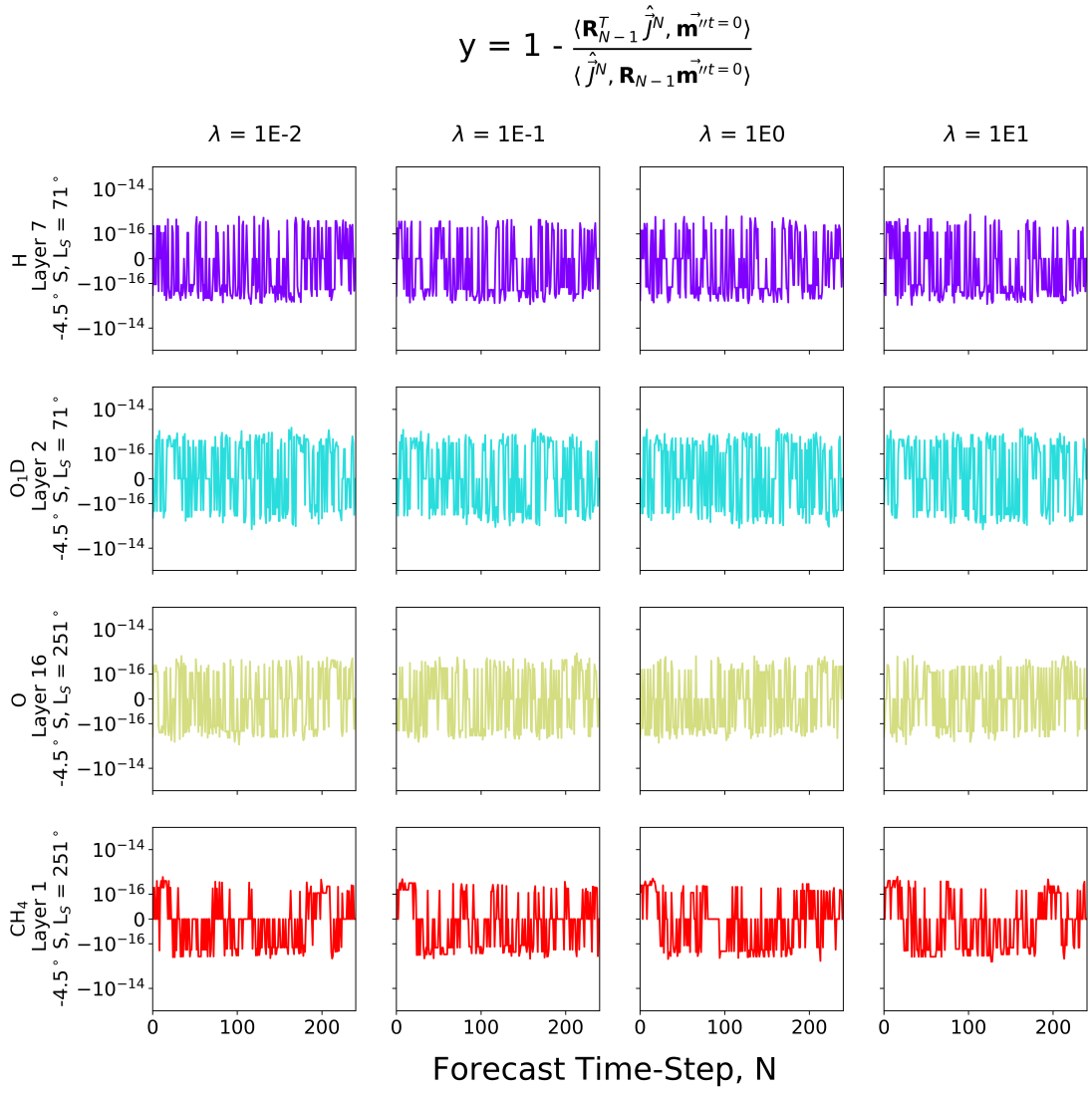

Figure S2: Adjoint property tests for each of the perturbation cases studied in Figure S1, using forecast elements as detailed on the left hand side. Each row corresponds to the respective test studied in Figure S1.

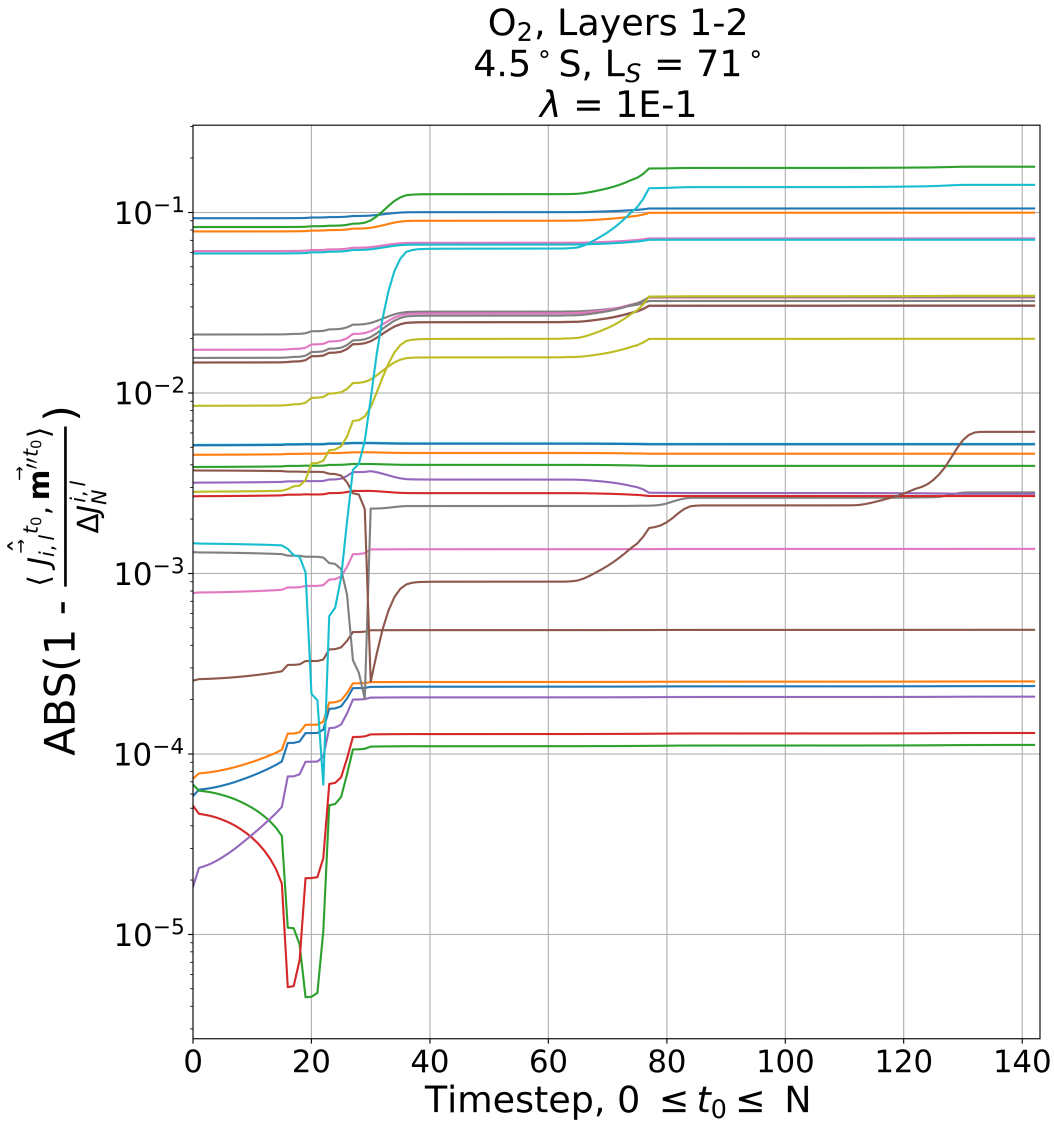

Figure S3: Temporal invariance of adjoint results. Each line corresponds to a model element with a forecast timestep perturbation value, $\Delta J_N^{i,l}$, greater than 10^{-16} kg/kg calculated via the adjoint equation, and its variance with respect to the 1-D model calculated value of $\Delta J_N^{i,l}$.

References

1. G. L. Mellor, T. Yamada, *Reviews of Geophysics and Space Physics* **20**, 851 (1982).

2. F. Forget, *et al.*, *Journal of Geophysics Research* **104**, 24155 (1999).

3. B. M. Taysum, P. I. Palmer, *Journal of Geophysical Research: Planets* **125**, e2020JE006491 (2020).

4. M. G. Trainer, *et al.*, *Journal of Geophysical Research: Planets* **124**, 3000 (2019).

5. A. C. Vandaele, *et al.*, *Space Sci. Rev.* **214**, 80 (2018).

6. O. Korablev, *et al.*, *Space Sci. Rev.* **214**, 7 (2018).

7. C. R. Webster, *et al.*, *Science* **360**, 1093 (2018).

8. S. D. Guzewich, *et al.*, *Journal of Geophysical Research (Planets)* **122**, 2779 (2017).

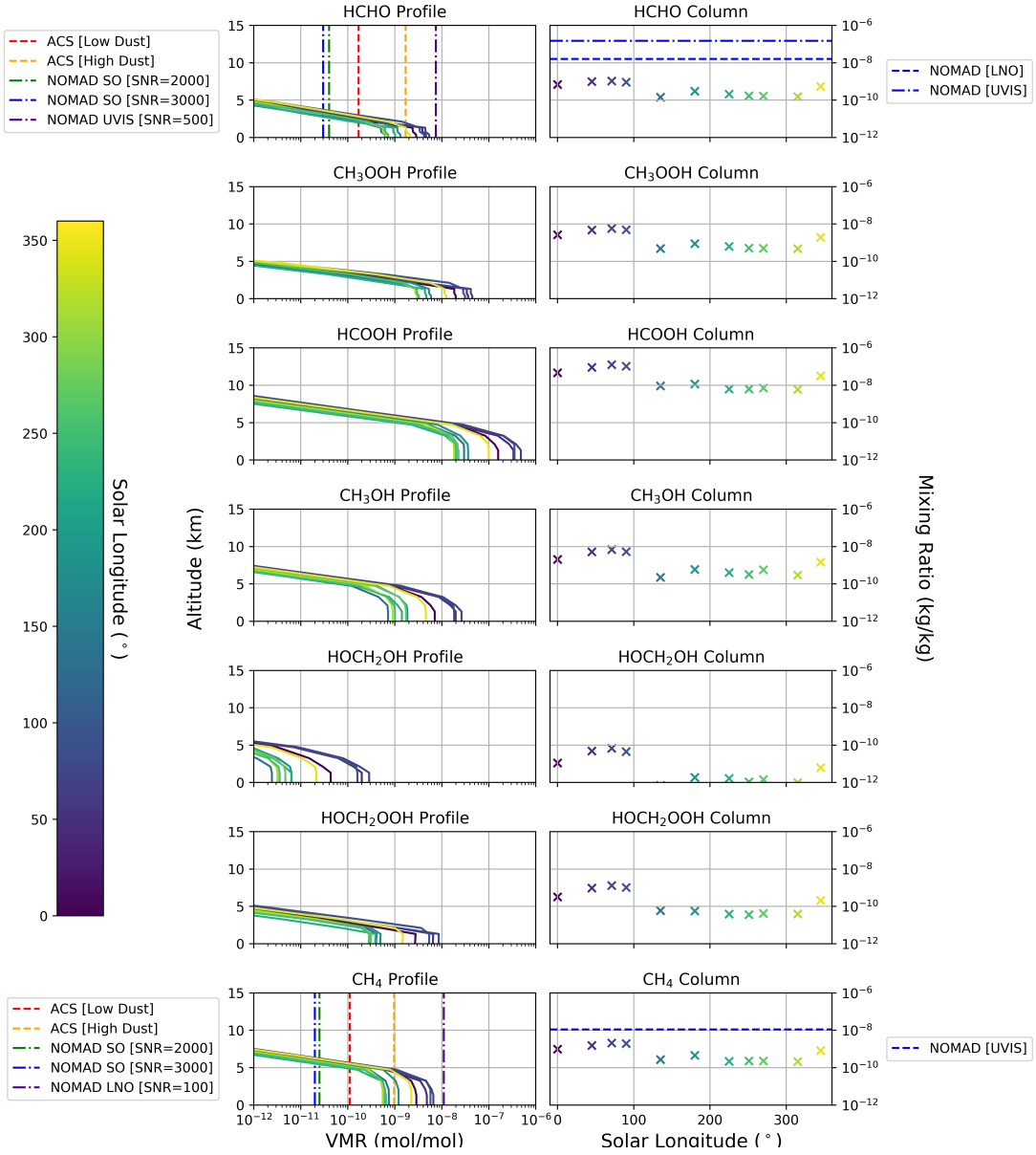

Figure S4: 1-D model organic products when initialised with SAM measurements of CH_4 concentrations at the surface, and a CH_4 photochemical lifetime forced to one hour below 400 m. Also shown are the theoretical detection limits of the ACS and NOMAD spectrometers aboard the ExoMars Trace Gas Orbiter, capable of measuring CH_4 and HCHO in solar occulation (profile) and nadir (column abundance) viewing modes.